JOURNAL OF GEOPHYSICAL RESEARCH, VOL. 104, NO. C8, PAGES 18,127–18,140, AUGUST 15, 1999

Cyclogenesis in the deep ocean beneath the Gulf Stream 2. Dynamics

Dana K. Savidge and John M. Bane Jr.

Department of Marine Sciences, University of North Carolina, Chapel Hill

Abstract. Strong cyclones in the deep ocean beneath the Gulf Stream have been observed during the period June 13, 1988, to August 7, 1990, near 68°W, 37°N in data from the Synoptic Ocean Prediction (SYNOP) Experiment. These cyclones developed in association with the evolution of large amplitude, quasi-stationary meander troughs in the Gulf Stream. It is likely that baroclinic instability is responsible for cyclone spin-up. The dynamical analysis of these cyclones indicates the process is analogous with atmospheric cyclogenesis from the perspectives of divergence and conservation of potential vorticity, but not in terms of the density field evolution. Large positive vertical velocities in the thermocline over developing low pressure centers at 3500 m are consistent with convergence at depth and divergence in the upper ocean, and with stretching of the lower water column and shortening of the upper water column. The stretching of the lower water column accounts for the generation of positive relative vorticity there. However, the evolution of the density field in the oceanic case does not resemble the atmospheric case. In the atmosphere, density field adjustments in the air column above the low pressure center at the Earth's surface are in the correct sense to account for decreasing pressure there. In the ocean, density field adjustments in the water column fail to account for the developing low pressure centers, so sea surface height depressions must be responsible. These depressions must have an approximate magnitude of 0.5 m depth over a 250 km horizontal extent (the cyclone's diameter).

1. Introduction

Strong coupling between the Gulf Stream and the underlying water column has been observed during the period June 13, 1988, to August 7, 1990, in the vicinity of 68°W, 37°N in data from the Synoptic Ocean Prediction (SYNOP) Experiment Central Array. The most conspicuous examples of this coupling are several strong cyclones in the deep flow that develop in association with the evolution of steep, large amplitude, quasi-stationary meander troughs in the Gulf Stream's path (Figures 1 and 2). Such well-organized, long-lived, energetic features have not been previously observed in the deep ocean so vividly. While strong velocities in the deep ocean near this location have been observed before [e.g., *Luyten*, 1977; *Hogg*, 1981], it was not until SYNOP that these flows were clearly seen to be part of well-organized mesoscale cyclones, strongly coupled to the evolution of the Gulf Stream path structure in the upper ocean. During the tenure of the SYNOP Central Array moorings, six well-defined instances of meander trough amplification and deep cyclogenesis occurred. *Savidge and Bane* [this issue] provide a description of these energetic events. The cyclones were characterized by strong swirl speeds (up to 0.5 m s^{-1}) and were long-lived (typically lasting 6-9 weeks) frequent occurrences (present 35% of the time during the 26 month deployment period). The strong cyclonic flows observed in the SYNOP Central Array at 3500 m extended throughout essentially the entire water column, from the benthic boundary layer, through the thermocline to the ocean's surface.

Meteorologists have studied similar flow features in the atmosphere for many years. Synoptic scale cyclones and anticyclones at the Earth's surface are known to be associated with waves in the jet stream in the upper troposphere and lower stratosphere. The three-dimensional evolution of these features is typically attributed to baroclinic instability, and their kinematics and dynamics are illucidated at length in atmospheric texts and literature [*Palmen and Newton*, 1969; *Bjerknes and Holmboe*, 1944; *Pedlosky*, 1987; *Gill*, 1982; *Holton*, 1979]. A particularly clear exposition of the mechanism of baroclinic instability from the perspective of conservation of potential vorticity is given by *Cushman-Roisin* [1994] and for the reader's convenience is briefly reviewed here. Consider a two-layer fluid on an f plane with an interface sloping downward from north to south. Suppose there is some northward fluid displacement in the upper layer. To conserve potential vorticity, such a displacement would imply shortening of the fluid column as it moved into the region of shallower interface depth, requiring the generation of negative relative vorticity, or the depression of the interface locally to conserve column depth. Some of each can

Paper number 1999JC900131.
0148-0227/99/1999JC900131$09.00

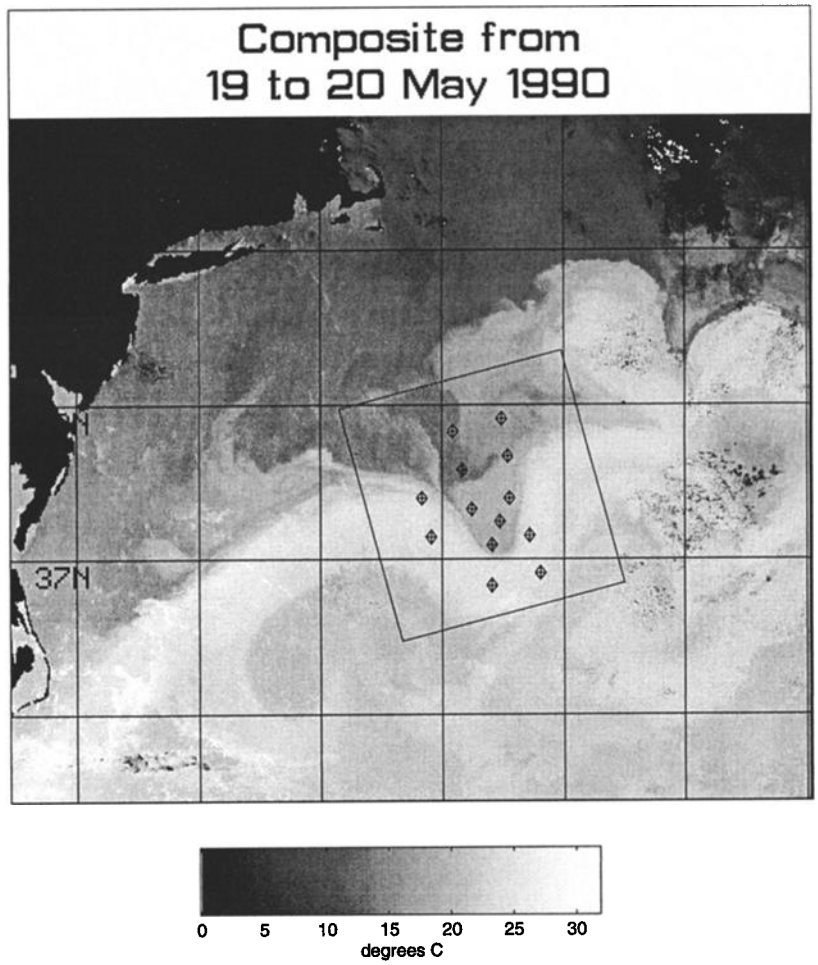

Figure 1. Composite image of satellite advanced very high resolution radiometer sea surface temperature for May 19-20, 1990. The image shows an example of a steep meander trough in the SYNOP Central Array. Also shown are the locations of the tall current meter moorings in the Central Array (diamonds with crosses) and the area (box) over which the depth of the 12°C isotherm can be optimally interpolated from the inverted echo sounders deployed in the Central Array. This box is the same area covered by the figures to follow (except Figure 5). (Image prepared by the P. Cornillon group of Univ. of Rhode Island.)

be expected to occur. Note that the sense in which the interface depth is being altered is consistent with lowering the potential energy of the two layer fluid. The depression of the interface depth would cause the underlying column of water to shorten and would likewise require the generation of negative relative vorticity there. The velocities thus generated in each layer could then cause further displacements of water in each layer. Displacements originating in the bottom layer can likewise initiate vorticity and further displacements in both layers. If sinusoidal displacements to the north and south along an east-west axis are assumed in each layer, motions in each layer can constructively or destructively interfere with motions in the other layer, such that the sinusoidal disturbances can propagate, amplify, or decay, depending on the offsets in the disturbances between layers. In the case where upper-layer displacements lead lower-layer displacements by a quarter wavelength in the direction of the basic flow in the upper layer, the disturbance in both layers will amplify.

Work in the early to middle 20th century on diagnosis of atmospheric cyclogenesis utilized the three-dimensional pressure fields, and it continues to be useful to understand the requirements on those fields during cyclogenesis. The displacement pattern leading to amplification for the two-layer case is consistent with the upper-level pressure field lagging the lower-layer pressure field by a quarter wavelength [*Cushman-Roisin*, 1994]. The lag may be less for the case of continuous stratification. In addition to the offset in the pressure field in the vertical, the pressure fields for the case of continuous stratification are surface intensified, consistent with closed low pressure fields at the Earth's surface and wavelike patterns in the upper troposphere and lower stratosphere [*Charney*, 1947; *Eady*, 1949]. Developing low pressure centers are characterized by convergent flow (see section 4), especially to the east of cyclone centers, while downstream from upper level trough axes, divergent flow is expected [*Bjerknes and Holmboe*, 1944]. Developing low pressure at the surface requires net decreasing den-

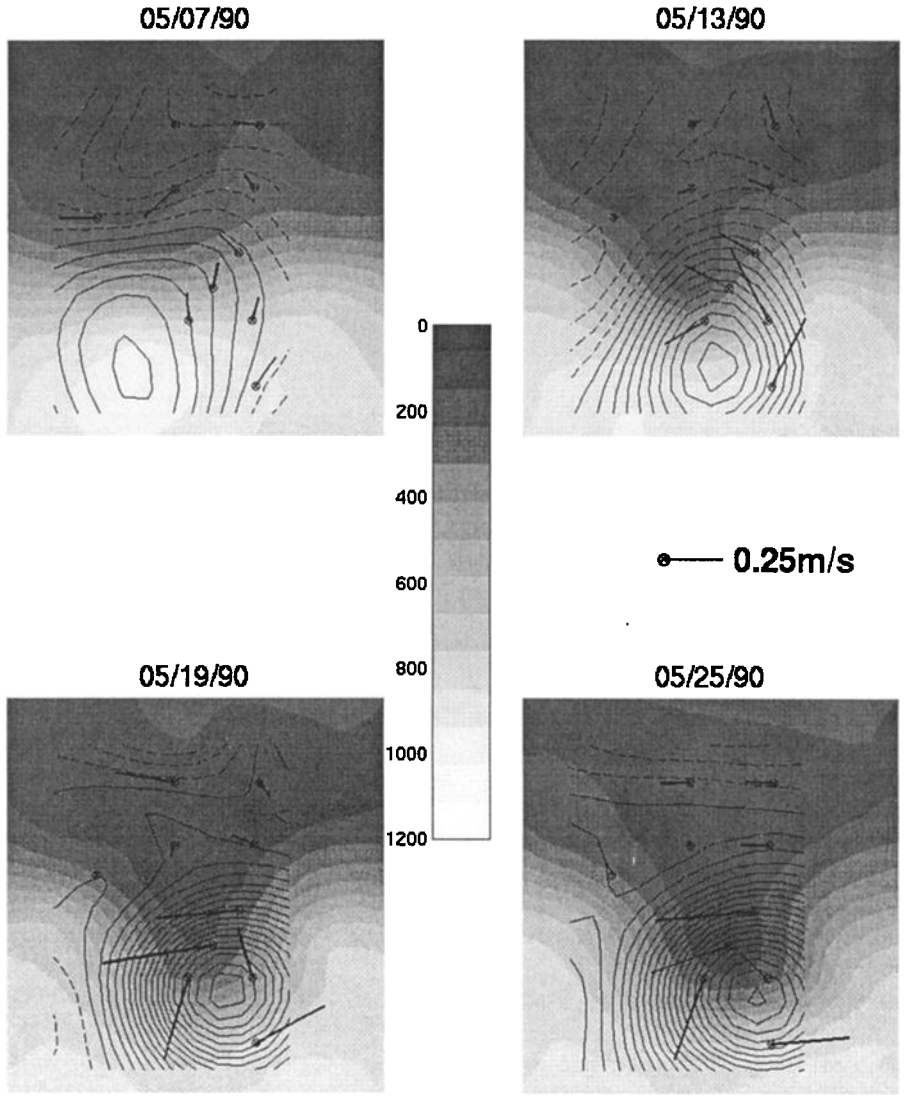

Figure 2. Time series of horizontal maps of data from the SYNOP Central Array at 6 day intervals, over an approximately 300 by 300 km area. These maps show the development of a steep meander trough in the Gulf Stream and a strong cyclone at 3500 m. The gray scale field represents the depth of the 12°C isotherm. The Gulf Stream jet closely follows the portion of the thermocline that slopes steeply from 200 to 800 m depth in the middle 1/3 of the array. The 13 current meter moorings of the Central Array are shown as circles with crosses. Vectors represent measured velocities at 3500 m. The contoured field is the optimally interpolated perturbation pressure field at 3500 m. Contour interval is 2×10^2 Pa (0.02 dbar); solid lines indicate negative values.

sity and net horizontal divergence in the air column above, further emphasizing the need for a downstream offset of the surface pressure field. Upward vertical motion is thus expected above surface lows, between the surface and the level of maximum horizontal divergence aloft. Finally, the pressure fields at all levels evolve in time, as the redistibution of the density fields by the three-dimensional velocity field progresses. As a consequence, the offset between surface and upper-level low pressure features is expected to decrease over time.

Oceanic cyclogenesis might be expected to be quite similar to atmospheric cyclogenesis. The two fluid media behave according to very similar sets of governing equations, and comparisons between the two using relevant nondimensional measures indicate dynamic similarity in many systems of interest [*Gill*, 1982; *Pedlosky*, 1987]. However, the two media do differ in their potential density distributions. The ocean is characterized by very small potential density variations relative to its average potential density. The atmospheric potential density field varies over its entire magnitude. In the ocean, those variations are concentrated over a very short interval in the vertical, namely the permanent thermocline, such that the ocean is often considered to be a two-layer system. The atmosphere's potential density variability is much more uniform in the vertical. The tropopause, about which the polar jet stream is approximately centered in the vertical,

marks the boundary between a region of almost linear temperature decrease with height (the troposphere) and a region of almost uniform temperature (the stratosphere). And finally, the ocean surface is characterized by a very large density interface, such that very small vertical displacements of the sea surface can result in very large horizontal pressure gradients. No such abrupt interface exists at the top of the atmosphere, where the density gradually approaches zero. Since baroclinic instability depends on the evolution of the density field, the differences in those fields between the two media suggest some variation in cyclogenesis between the ocean and the atmosphere is possible.

In order to initiate a comparison between atmospheric and oceanic cyclogenesis, the dynamics of the ocean cyclones are examined in the following. A variety of dynamical viewpoints are utilized, including linear momentum, divergence, and vorticity balances. While the study of atmospheric cyclogenesis has progressed far beyond the simple diagnoses performed below, the early work in that field showed the causes of the evolution of the observed fields quite clearly. It seems appropriate to begin at the beginning with oceanic cyclogenesis as well, especially considering that the vertical sparcity of this data set makes the application of modern atmospheric techniques impossible. The different components of this study paint a consistent story of cyclone spin-up, in most ways analogous to atmospheric cyclogenesis, but with some departures from that analogy.

2. Data and Data Products

The data used here were acquired as part of the SYNOP Experiment. The observational component of this study included four mooring arrays along the Gulf Stream mean path downstream of Cape Hatteras, several hydrographic cruises, isopycnal RAFOS float deployment, and the acquisition of satellite measurements of sea surface temperature. This study uses data from the SYNOP Central Array, located over an approximately 300 by 300 km area centered at 37.5°N, 67.5°W. This array consisted of 12 tall current meter (CM) moorings with velocity (speed and direction converted to Cartesian coordinate components u and v), temperature (T), and pressure (p) sensors at target depths of 400, 700, and 1000 m, velocity and T sensors at 3500 m, and with bottom pressure sensor and inverted echo sounder (IES) moorings colocated with the 12 CM moorings. An additional ring of 13 bottom mounted IES moorings encircled the 12 central moorings (Figure 1). The complete array was in place from May 1988 through August 1990, a period in excess of 2 years. A 13th CM mooring was deployed during the second half of this period. Details on the processing of the Central Array data are given by *Savidge and Bane* [this issue].

3. Pressure Tendency

The rapidly deepening low pressure centers observed at 3500 m with which the large cyclonic velocities are associated are a primary feature of the deep cyclones. A diagnosis of how the pressure falls at a given location was made using what will be called the pressure tendency equation, as in *Bjerknes and Holmboe* [1944]. This equation is the hydrostatic equation integrated over depth and differentiated with respect to time:

$$\underbrace{\frac{\partial p_{z_0}}{\partial t}}_{a} = \underbrace{\rho g \frac{\partial \eta}{\partial t}}_{b} + \underbrace{g \int_{z_0}^{\eta(t)} \frac{\partial \rho}{\partial t} dz}_{c} \tag{1}$$

where p_{z_0} is the pressure at 3500 m. Leibnitz' rule must be used in order to bring the partial with respect to time inside the integral on the right-hand side, since the upper limit of integration, η, the sea surface height, is a function of time. This results in the $\partial\eta/\partial t$ term on the right-hand side. For the atmospheric case, the hydrostatic equation is integrated upward to infinity, where p and ρ both approach zero, so no such upper surface variability term exists. The terms of equation (1) contributing to the change in pressure at 3500 m with time (term a) represent vertical movement of the sea surface (term b), and the net effect of changing density in the water column above 3500 m (term c), to be referred to here as "the integrated density tendency" effect.

3.1. Estimates of Tendency Terms

Quantitative assessments of terms a and c in equation (1) have been made using SYNOP data. Estimates of the temporal change in pressure at 3500 m ($\partial p_{z_0}/\partial t$) were made as first differences in the OI pressure perturbation fields at 3500 m. During developing days of the cyclone events, $\partial p_{z_0}/\partial t$ was consistently negative (Figure 3a) in the vicinity of cyclone centers. The developing low pressure features eventually reach values of up to about -4×10^3 Pa (-0.4 dbar). Note the clear downstream offset between the axis of the large amplitude meander trough in the upper ocean and the low pressure center at 3500 m. This offset is also evident in Figure 2.

Density values at the measurement levels were calculated from the measured temperatures as described by *Savidge and Bane* [this issue], utilizing the North Atlantic salinity algorithm of *Armi and Bray* [1982]. The vertically integrated density tendency term was estimated by taking first differences in time of the OI density fields at each of the four measurement levels and then crudely integrating in the vertical by weighting each level by the portion of the water column it is presumed to represent, summing, and multiplying by g. Estimates at the 3500 m level were assumed to hold over 2000 m; the remaining three levels hold over 300 m each. The integrated density tendency was consistently positive during developing days of cyclones near cyclone centers (Figure 3b). The veracity of the crude integration scheme is supported by the fact that density increases were seen at all measurement levels near cyclone centers (not shown). This leads to the conclusion that the falling pressure at 3500 m during cyclone spin-up cannot be accounted for by the integrated density tendency term on the right-hand side of equation (1): it must be the result of a falling sea surface. This topic will be discussed further in section 3.2.

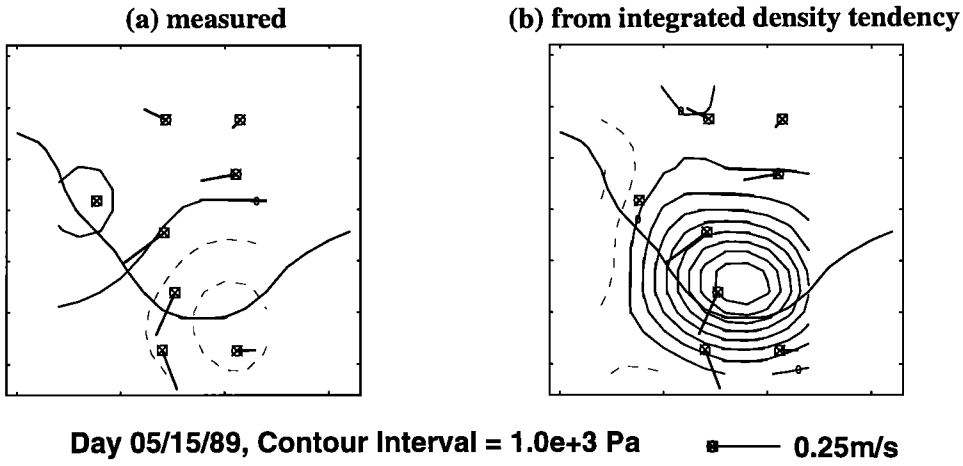

Figure 3. The change in pressure at 3500 m that occurred over the first 15 days of deep cyclone event C. (a) Measured (term a in equation (1)) and (b) from integrated density tendency (term c in equation (1)). Solid contours represent zero or positive values; dashed contours are negative. The contour interval is 1.0 x 10^3 Pa (0.1 dbar). The single bold line crossing the pressure contours is the 400 m contour of the depth of the 12°C isothermal surface, indicating the approximate path of the Gulf Stream jet. Vectors are measured velocities at 3500 m.

The bull's-eye pattern approximately centered in the developing Gulf Stream trough is consistent with the increasing curvature and southward migration of the Gulf Stream in the Central Array, as seen in satellite imagery, and the resultant local shoaling of the thermocline as the Gulf Stream and its associated thermal structure moved past the moorings. Since the migration in this case is accompanied by a large increase in Gulf Stream path curvature, it is suggestive of baroclinic instability. That process depends on, in fact is defined by, a redistribution of the density field in the jet itself. That redistribution is accomplished by the three dimensional velocity field in the jet, which varies from the mean jet structure, and includes ageostrophic components that may be large in relation to the translation velocity of the Gulf Stream over the array [*Howden*, 1996]. Therefore the components of the integrated density tendency term during the trough amplification phase could contain interesting information about the trough amplification and deep cyclone development.

The integrated density tendency term can be broken down into components, starting with the thermodynamic equation differentiated with respect to time [see *Gill*, 1982, section 3.6]

$$\begin{aligned}\frac{d\rho}{dt} &= \frac{\partial\rho}{\partial t} + \mathbf{V}\cdot\nabla\rho \\ &= \left(\frac{\partial\rho}{\partial p}\right)_{T,S}\frac{dp}{dt} + \left(\frac{\partial\rho}{\partial T}\right)_{p,S}\frac{dT}{dt} \\ &= -\frac{g\rho^2 w}{\kappa_s} + \alpha\rho\Gamma w\end{aligned}$$

This can be solved for the local change of density with respect to time to get

$$\underbrace{\frac{\partial\rho}{\partial t}}_{a} = \underbrace{-\mathbf{V_h}\cdot\nabla_h\rho}_{b} \underbrace{- w\frac{\partial\rho}{\partial z}}_{c} \underbrace{- \frac{g\rho^2 w}{\kappa_s}}_{d} + \underbrace{\alpha\rho\Gamma w}_{e} \qquad (2)$$

Here $\mathbf{V}$ and $\mathbf{V_h}$ are the total and horizontal velocities, $\kappa_s = \rho/(\partial\rho/\partial p)$ is the secant bulk modulus, $\alpha = -\frac{1}{\rho}(\partial\rho/\partial T)_{p,S}$, $\Gamma = -(gT)/(c_p\rho)(\partial\rho/\partial T)_{p,S}$, and c_p is the specific heat of seawater at constant p. The terms contributing to the change in density through the water column with time (term a) represent horizontal advection of the density field (term b), vertical advection of the density field (term c), the effect of changing pressure on density (term d), and the effect of adiabatic temperature change on density (term e). The version of this equation used in the atmosphere has an additional right-hand side term representing density changes due to latent heat release through state changes (precipitation).

The development of the pressure fields in the atmosphere consistent with jet stream trough amplification and cyclone spin-up is clearly shown by *Fleagle* [1948] (or see [*Palmen and Newton*, 1969, Figure 6.4]). The pressure field at any particular level is determined by the weight of the air column above it, which is determined by changes in the density field in that column. In the case of atmospheric cyclogenesis through baroclinic instability, that field alteration occurs primarily as a result of horizontal advection of density. Vertical motions consistent with the variation in horizontal convergence in the vertical can also contribute to alteration of the density field, primarily through thermodynamic effects.

In oceanic cyclogenesis, unlike in atmospheric cyclogenesis, the evolving density field does not account for the pattern of developing pressure fields at 3500 m depth. However, a comparison of horizontal advection patterns in the ocean with those in the atmosphere will help to make clear the similarities between the two systems. Horizontal advection of the density field can be calculated from vertical shear. That shear vector is the thermal wind, which blows parallel to isopycnals, such that if the total velocity turns with height, it flows across isopycnals and advects density horizontally. Vertical shear was determined from the horizontal density gradient using the thermal wind equation. Estimates of ve-

locity 1 m above the measurement levels $\mathbf{V}_{+1} = (u_{+1}, v_{+1})$ were calculated by adding shear vectors from thermal wind shear estimates $\mathbf{V}_{sh} = (\frac{\partial u}{\partial z}\triangle z, \frac{\partial v}{\partial z}\triangle z)$ to the optimally interpolated velocities at measurement levels $\mathbf{V}_{OI} = (u_{OI}, v_{OI})$. Both $\mathbf{V}_{OI}$ and $\mathbf{V}_{+1}$ were converted to magnitudes and directions, and differences were taken to calculate turning due to thermal wind shear, θ. That angle in radians can then be converted to an estimate of horizontal advection of density according to: $\mathbf{V}_H \cdot \nabla_H \rho = -|\mathbf{V}_{OI}| \frac{f_0}{g} \times \theta$ [*Bluestein*, 1992]. The sign of these calculations, and thus of the warm/cold advection, is considered robust, since it depends primarily on shear estimates calculated from the density field. The shear vectors $\mathbf{V}_{sh}$ are typically oriented several tens of degrees from the direction of $\mathbf{V}_{OI}$ so that the errors in the directions of the measured and shear vectors must sum to tens of degrees in order for the sign of the estimated turning to be incorrect. Such large errors are not expected. Only the signs of these calculations are plotted and discussed in this section.

The velocities turned clockwise with height downstream from Gulf Stream troughs at all four measurement levels. This "veering" is associated with the horizontal advection of warm water (warm advection) (Figure 4). This would contribute to decreasing density in the water column above the low pressure centers at 3500 m, consistent with the development of that low but in contrast to the increasing densities actually observed. Conversely, the velocities upstream from Gulf Stream troughs turned counter-clockwise with height downstream from Gulf Stream troughs at all four measurement levels. This "backing" is associated with the horizontal advection of cold water (cold advection) (Figure 4). Magnitudes of horizontal density advection at the upper three levels typically exceeded those at 3500 m by approximately tenfold, consistent with the very small horizontal density gradients found in the subthermocline ocean. These thermal wind calculations are consistent with those made as finite difference estimates of the vertical shear calculated from the measured and optimally interpolated velocities at measurement levels. They are consistent with the sense of the vertical velocities seen upstream (downward) and downstream (upward) from trough axes (to be discussed) in the upwelling, veering, warm advection (uvw) and backing, cold advection, downwelling (abc) sense discussed by *Bluestein* [1992] and *Lindstrom et al.* [1997]. If indeed baroclinic instability is acting and ageostrophic velocities are crossing isopycnals in the correct sense to decrease mean potential energy, then they are also consistent with the ageostrophic velocity field seen by *Howden* [1996] in the Gulf Stream jet in amplifying troughs and with the residual fields of velocity calculated by *Savidge and Bane* [this issue].

Horizontal advection effects are in the wrong sense to account for the total integrated density tendency during cyclo-

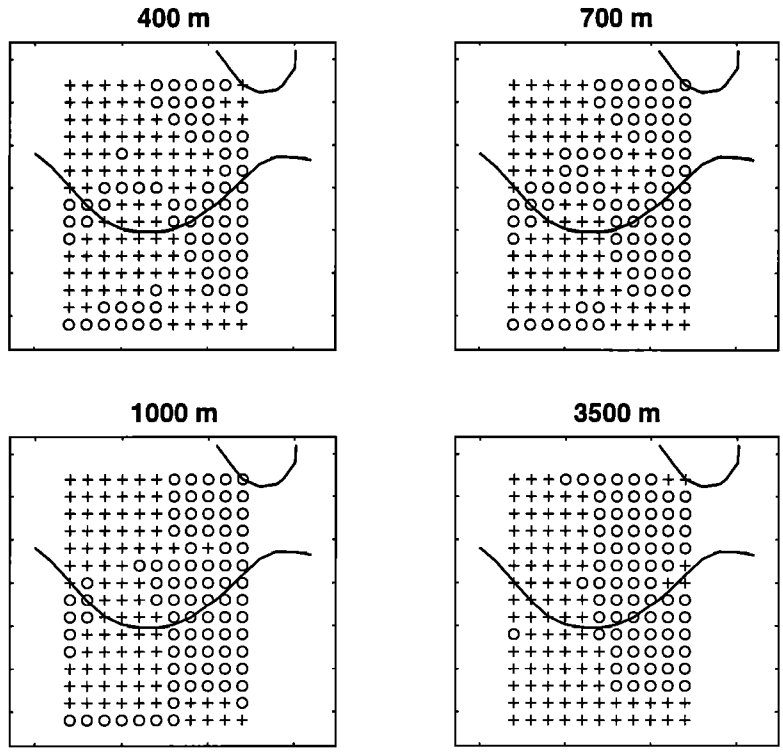

Figure 4. Horizontal maps of the sign of horizontal advection integrated over the first 6 days of event A. Estimates are from thermal wind turning, using optimally interpolated data at the four measurement levels. Crosses indicate cold advection; open circles indicate warm advection. The bold lines are 400 m depth contours of the 12°C isothermal surface, indicating the approximate path of the Gulf Stream jet across the array and a warm core ring in the northeastern corner of the array.

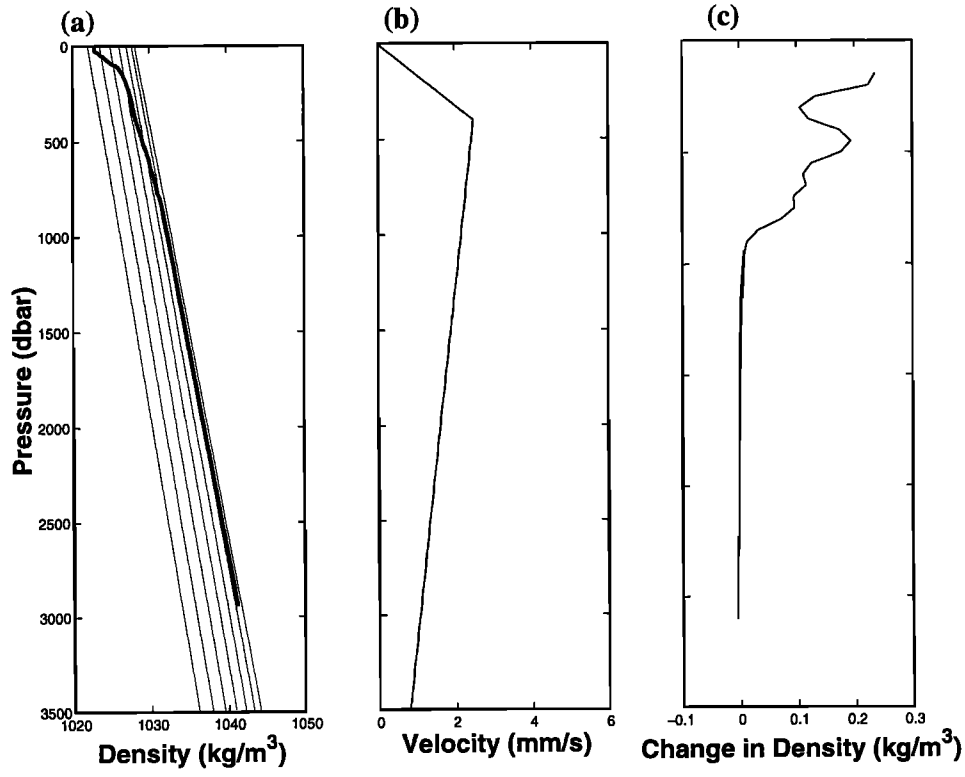

Figure 5. The effect of vertical motion on the integrated density tendency term during cyclogenesis. (a) A vertical profile of potential density through the Gulf Stream overlain on potential density contours for ocean water. These values were calculated using the seawater routines of *Morgan* [1994] for source water at 4000 m, salinity of 35, and in situ temperature of 0°-30°C at 5°increments. (b) A vertical velocity profile representative of a location near the Gulf Stream axis, downstream from a developing meander trough axis. (c) The profile of density difference resulting from advecting the density profile in a by the vertical velocity profile in b for 1 day.

genesis, so the effects of the remaining terms in equation (2) must dominate. Terms d and e in equation (2) are essentially vertical motion effects, as is term c in equation (2), since the temperature of a water parcel in the interior of the ocean and the pressure field it experiences are primarily altered by moving it vertically. The total effect of vertical motion on the pressure tendency at 3500 m during cyclone events can be anticipated by considering a vertical profile of density in and below the Gulf Stream (Figure 5a). This density profile was calculated from temperature, salinity, and pressure information from a conductivity-temperature-depth cast taken in the middle of the Gulf Stream at about 74°W *Savidge et al.* [1993]. It is superimposed on the adiabatic temperature gradient in the ocean, calculated as the potential density of water at 4000 m ($p = 4000$ dbar, $S = 35$ practical salinity unit, $T = 0°$-30°C) referenced to decreasing depths, up to the sea surface. In the deep ocean the in situ density profile is very nearly adiabatic, so vertical motion there would contribute little to the integrated density tendency. In the thermocline, however, the density gradient is not adiabatic, so that vertical motion there could result in a net change in the integrated density tendency, since there term c outweighs terms d and e in equation 2. A sample vertical profile of upwelling vertical velocity is shown (Figure 5b), and it was used to assess the effect of vertical advection of water of the density indicated (Figure 5a) for 1 day. The density of the water at its new level was calculated and compared to the original profile, and a density difference was calculated. The resulting profile of the net effect of vertical motion over 1 day shows very little effect in the deep ocean, but shows large increases in density in the thermocline, where both the vertical velocities and the difference between the adiabatic and the in situ density gradients are large (Figure 5c). A simple trapezoidal integration of this density difference over depth multiplied by g indicates a net increase in pressure beneath the column of nearly 1000 Pa (0.1 dbar) in just 1 day. Clearly the vertical motion effects can be of sufficient magnitude to explore further.

Lindstrom et al. [1997] have shown large vertical velocities in the thermocline during periods of Gulf Stream trough amplification and deep cyclogenesis. Their calculations were made using the SYNOP data and the heat equation and were shown to be in good agreement with the vertical velocities indicated by coincident RAFOS floats. They show positive vertical velocities downstream from trough axes, with typical values in the central portion of the developing cyclones of 2-4 mm s^{-1}, persisting for $\simeq$10 days or more. Using their vertical velocities, calculations of the ver-

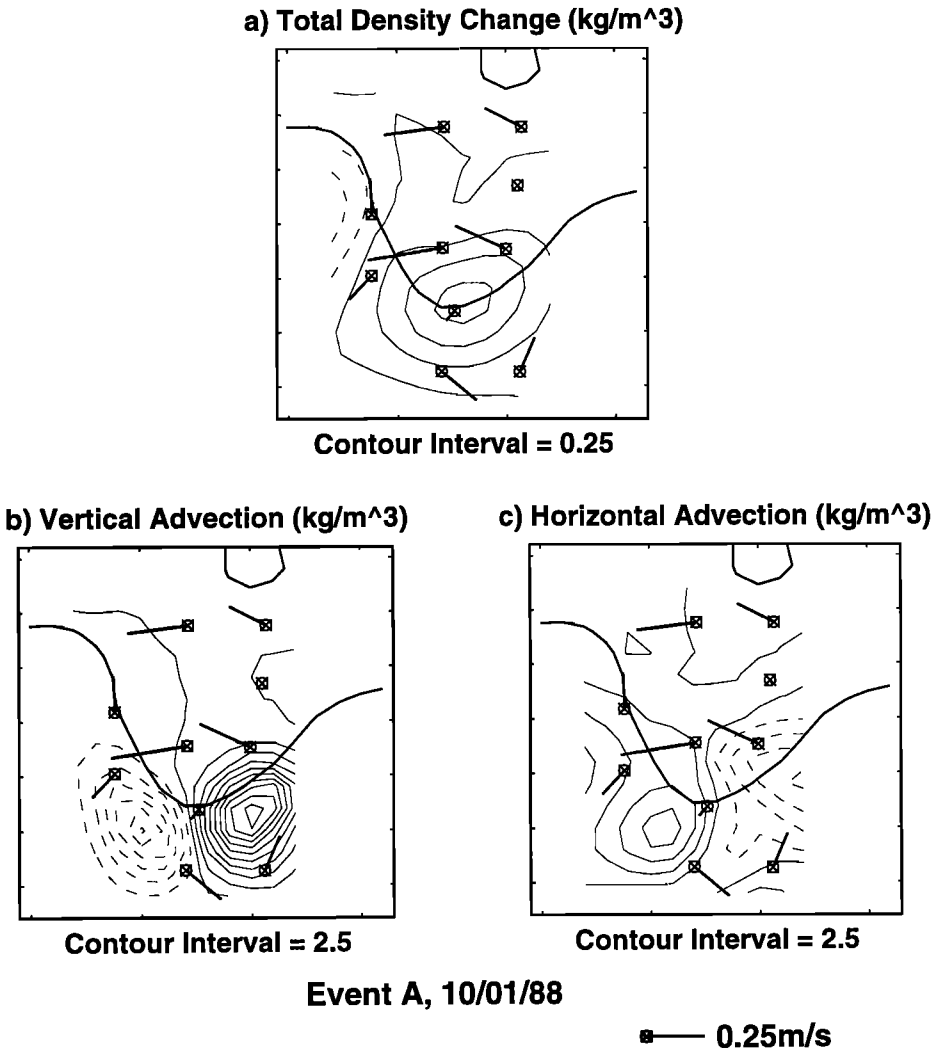

Figure 6. Advective components of the integrated density tendency term at 700 m, integrated over the first 15 days of event A. (a) Total measured density change, (b) vertical advection component, and (c) horizontal advection component, calculated from thermal wind shear. The bold lines are 400 m depth contours of the 12°C isothermal surface, indicating the approximate path of the Gulf Stream jet across the array, and a warm core ring in the northeastern corner of the array. Vectors are measured velocities at 3500 m, shown to indicate the deep cyclone.

tical advection of density were made here. The vertical gradient in potential temperature at 400 m depth was calculated as a function of thermocline depth according to the methods of *He* [1993]. These gradients were converted to density gradients using the in situ temperatures, salinities calculated according to the *Armi and Bray* [1982] algorithm, as discussed by *Savidge and Bane* [this issue], and the equation of state for seawater [*Morgan*, 1994]. The sense of the resulting vertical density advection in the vertical is to increase density downstream from trough axes and to decrease density upstream from trough axes, as shown in Figure 6b for data integrated over the first 15 days of event A. The effect from horizontal advection is also shown (Figure 6c), as is the measured density increase over these developing days (Figure 6a). These estimates illustrate that there is a different balance on the right-hand side of equation (2) for oceanic cyclogenesis than for atmospheric cyclogenesis. In the atmosphere, the integrated density tendency in the air column determines the sense of the developing pressure features below and is dominated by horizontal advection at all levels. In the ocean, the integrated density tendency term is of the opposite sign than the pressure tendency term and is dominated by the vertical advection effect, despite horizontal advection that is consistent with the atmospheric case. Therefore the sea surface must fall to account for the falling pressures observed at 3500 m.

3.2. Sea Surface Height Term

In the mean, sea surface height (SSH) rises by about 1 m across the Gulf Stream in the offshore direction, while thermocline depth (Z12) increases by hundreds of meters in the same direction. The effects of these sloping surfaces on the pressure field below the thermocline are of approximately

equal (about 10^4 Pa or 1 dbar across the Gulf Stream) but opposite magnitudes, such that pressure gradients below the thermocline are typically very small in the absence of strong curvature in the Gulf Stream [see, e.g, *Savidge and Bane*, this issue, Figure 4.]. Southward migration of a straight Gulf Stream over the Central Array would presumably result in a locally falling SSH, locally shoaling Z12, and little apparent local change in pressure below the thermocline. However, in the case of meander trough amplification and deep cyclogenesis, the Gulf Stream's cross-stream sea surface and thermocline topography move southward across the Central Array as the result of the development of large curvature in the Gulf Stream itself. As a first approximation, it is likely that the evolution of the sea surface topography mirrors that of the thermocline topography (since whatever advects density does so by advecting the water itself), such that the development of large Gulf Stream curvature should be apparent in both fields. However, the development of such curvature through baroclinic instability proceeds through the slight rearrangement of the density field by the three-dimensional velocity field. This rearrangement occurs in such a way that the components of the subthermocline pressure fields due to the sea surface and thermocline topographies no longer cancel each other completely, and a large pressure deficit (up to 0.4×10^4 Pa or 0.4 dbar) develops in the deep layer downstream from trough axes. The pertinent question is, in what way does the evolution of the sea surface height topography not mirror that of thermocline depth topography exactly.

One possibility is that in addition to an in-phase offshore migration of both Z12 and SSH in a developing trough, there is a region downstream from the trough axis where divergent horizontal flow in and above the thermocline results in a depression in the sea surface that adds to the otherwise cross-stream sloping SSH. The magnitude of this depression would need to be large enough to account for the large low pressure center observed at 3500 m, or approximately 0.4 m depth. A schematic of this scenario is shown in Figure 7. A straight Gulf Stream exhibits SSH and Z12 contours that are essentially parallel to each other, with both SSH and Z12 increasing in the offshore direction (Figure 7a). The in-phase component of the SSH and Z12 trough migration is shown in the left side of Figure 7b. The hypothesized sea surface depression caused by horizontal divergence in the thermocline downstream from the trough axis is shown in the middle of Figure 7b, and the sum fields are shown in the right side of Figure 7b. Note that the result is an apparent downstream shift in the SSH trough, relative to the Z12 depth trough. This situation can be illustrated using SYNOP data from the interior of the ocean. If the horizontal structure of the temperature field is represented by Z12 depth and the SSH field is represented by the pressure field at 400 m (as calculated using optimal interpolation from velocities at 400 m and assuming geostrophy), we find essentially parallel temperature and pressure field contours for a nearly straight Gulf Stream but nonparallel contours with a downstream offset in the SSH trough axis in the case of an amplifying Gulf Stream meander trough (Figure 8).

4. Horizontal Divergence

If the sea surface is to fall locally over the developing low pressures observed at 3500 m, net divergence is required in the water column between the sea surface and 3500 m. While geostrophic and steady symmetric gradient wind balance flow are identically nondivergent, regions of developing circular cyclonic flow are associated with convergence [*Gill*, 1982]. Thus the developing deep ocean cyclones are expected to be convergent features. However, the upper ocean flow is not circular so the flow there will not necessarily be convergent and may supply the divergence required for

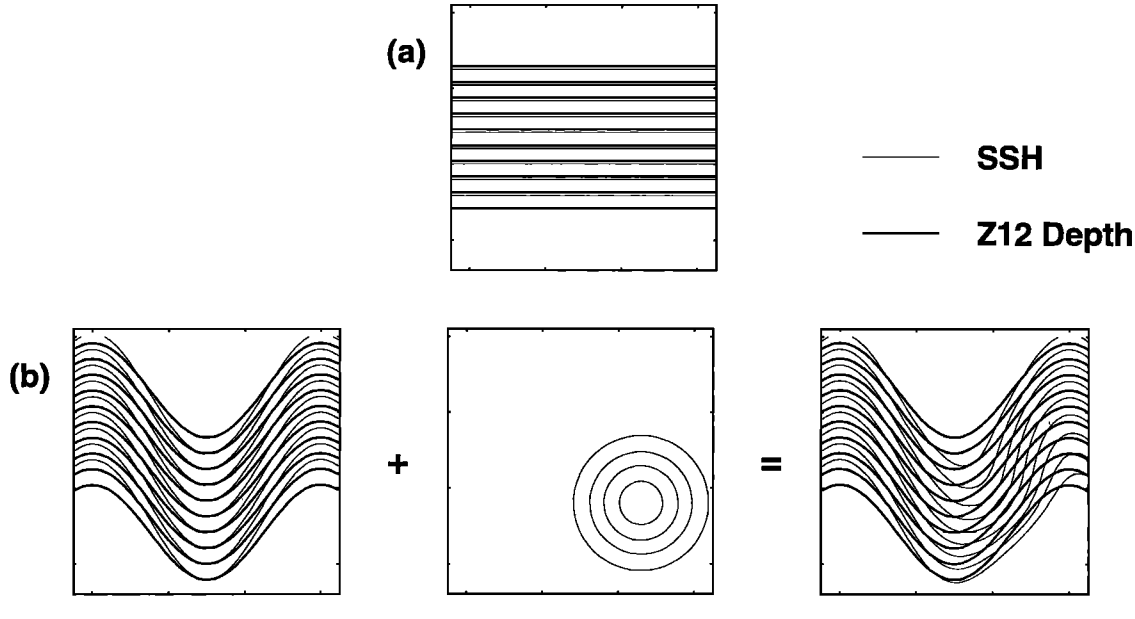

Figure 7. Schematic SSH and Z12 contours for (a) a straight Gulf Stream and (b) a curved Gulf Stream with deep cyclone. The thin lines represent SSH contours; the thick lines represent Z12 depth contours.

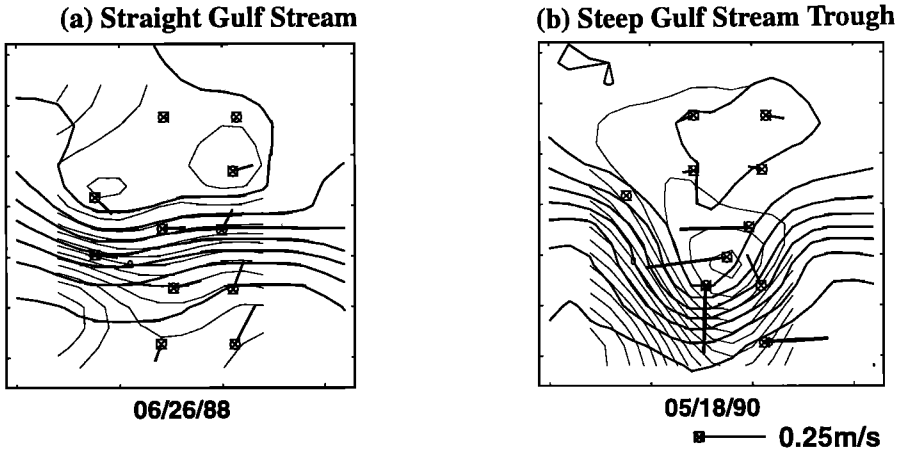

Figure 8. Depth of 12°C isothermal surface (bold lines, contour interval is 100 m) and pressure perturbation field at 400 m depth (thin lines, contour interval is 1.0 x 10^3 Pa (0.1 dbar)), calculated using optimal interpolation from measured velocities at 400 m assuming geostrophy, for (a) straight Gulf Stream and (b) developing Gulf Stream trough. Vectors are measured velocities at 3500 m.

the hypothesized developing sea surface depression. Divergence is expected in the atmosphere and the ocean between jet troughs and crests [*Bjerknes and Holmboe*, 1944; *Bower*, 1989]. In the following, the oceanic divergence situation is shown to be consistent with the atmospheric case.

The horizontal divergence is equal to vertical stretching, $-\partial w/\partial z$, according to continuity. Since vertical velocities near the Gulf Stream show a primarily first baroclinic mode structure [*Hall*, 1986; *Rossby*, 1987], vertical stretching in the deep ocean was calculated from vertical velocities at 700 m (calculated using the method of *Lindstrom et al.* [1997]) divided by the water depth between 700 m and the bottom. The implicit assumption of vanishing vertical velocity at the bottom is validated by potential vorticity estimates (section 5). Vertical stretching can be calculated for the upper 700 m of the water column from vertical velocities at 700 m ($\times -1$) divided by 700 m, assuming negligible surface vertical velocities. The sign of these calculations, which is of primary interest here, will be correct to the extent that (1) the signs of the [*Lindstrom et al.*, 1997] vertical velocities are correct and (2) the first baroclinic mode assumption is true. *Lindstrom et al.* [1997] place good confidence in those signs during cyclogenesis, based on independent estimates from RAFOS float trajectories. These divergence estimates indicate convergence in the deep ocean downstream from Gulf Stream trough axes (Figure 9a), and divergence in the upper layer during developing days. The magnitude of the convergence in the lower layer, O(0.5% f), is more than adequate to spin up the total relative vorticity of the cyclones observed there [*Savidge and Bane*, this issue], assuming a two-term balance between the divergence and $\partial\zeta/\partial t$. Divergence of O(5% f)in the upper layer is consis-

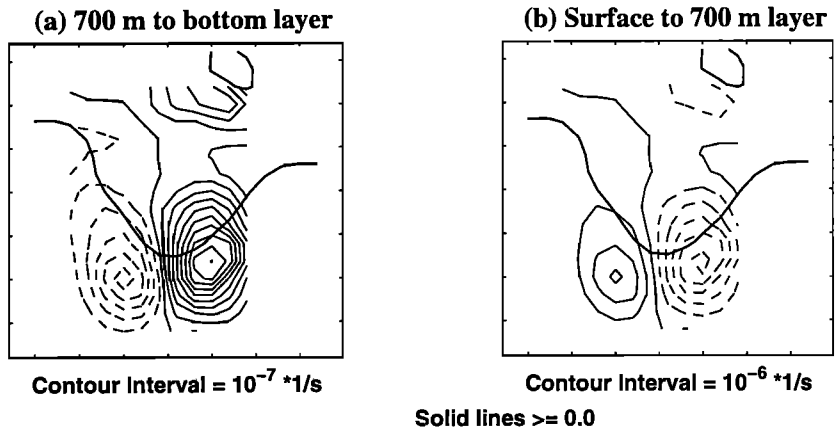

Figure 9. Divergence from water column stretching over the upper and lower water column integrated over the first 12 days in Event A. Maps are for layers from (a) 700 m to ocean bottom and (b) sea surface to 700 m. Positive values indicate convergence and production of positive relative vorticity. Note the difference in contour interval between the two. The bold lines are 400 m depth contours of the 12°Cisothermal surface, indicating the approximate path of the Gulf Stream jet across the array and a warm core ring in the northeastern corner of the array.

tent with independent vorticity estimates for a curved Gulf Stream as given by *Bower* [1989] and *Rossby and Gottlieb* [1998]. The large vertical velocities in the thermocline are due largely to cross-stream flow along the inclined isothermal surfaces [*Lindstrom et al.*, 1997]. This cross-stream flow is composed mainly of the barotropic cyclonic velocities evident at 3500 m and apparently extending up through the thermocline [*Savidge and Bane*, this issue; *Howden*, 1996].

The horizontal divergence can also be calculated from horizontal flow field information, as by *Gill* [1982]. The velocities in the inviscid equations of motion may be decomposed into geostrophic and ageostrophic parts and the equations solved for the ageostrophic parts. The horizontal divergence of the ageostrophic velocity field can then be calculated:

$$-\nabla_H \cdot \mathbf{V_a} = \frac{1}{f_0}\left(\frac{\partial \zeta_g}{\partial t} + \beta v_g + \mathbf{V_g} \cdot \nabla_H \zeta_g\right) \qquad (3)$$

Here $\mathbf{V_a}$ and $\mathbf{V_g}$ are the ageostrophic and geostrophic parts of the horizontal velocity field, v_g is the northward component of $\mathbf{V_g}$, ζ_g is the relative vorticity of the geostrophic flow, and f_0 and β are the Coriolis parameter at 37.5°N and the gradient of f with northward displacement. In the following, it is once again the sign that is of primary interest. While it would be interesting to examine magnitudes to see if upper level effects dominated lower level effects, any difference would be small relative to the terms at specific levels and quite difficult to calculate or to integrate in the vertical to the accuracy necessary to make such a net estimate. However, the signs of these calculations should be correct based on the following: For the increasingly cyclonic circular flow in the deep ocean associated with cyclone spin-up, convergence is expected, since the advection of planetary vorticity and relative vorticity are expected to be second-order effects early in the development of such flow [*Holton*, 1979]. Estimates of ζ using OI and SYNOP OI velocities should have the correct sign near cyclone centers, given the robustness of the cyclones' radial structure seen by *Savidge and Bane* [this issue]. First differences in time of ζ should similarly have the correct sign, given the steady increase in velocities seen at 3500 m and the increasing steepness of the velocity versus radius curve with time over developing days. The signs of the calculations in the upper ocean are less certain, given the competing contribution from the advection of ζ term. However, the calculations are consistent with the stretching estimates. They are also consistent with Gulf Stream vorticity analyses of *Bower* [1989] and *Rossby and Gottlieb* [1998] and with what is expected from atmospheric cyclogenesis. Away from mooring locations, of course, the signs and magnitudes of the calculations at both levels are increasingly suspect.

Divergence was calculated from the right-hand side of equation (3) and SYNOP OI velocities and relative vorticities. The OI estimates are constrained to be nondivergent and are composed mainly of a geostrophic component, together with a small, nondivergent, nongeostrophic component [*Howden*, 1996]. These calculations indicate net convergence near and to the east of cyclone centers at 3500 m (Figure 10a), primarily due to the relative vorticity tendency term, $\partial\zeta/\partial t$. Advection of relative vorticity can become large by the midlife of cyclone events (components not shown). At 400 m, convergence and divergence values are quite large (note contour interval change from Figures 10a to 10b), usually with predominantly divergent areas located immediately downstream from trough axes during cyclone development. At this upper level, where the total flow is not circular, the magnitude of relative vorticity advection becomes as large or larger than the relative vorticity tendency (components not shown). Advection of planetary vorticity remains negligible, as it was at 3500 m. These divergence estimates are consistent with those made from vertical stretching (Figure 9).

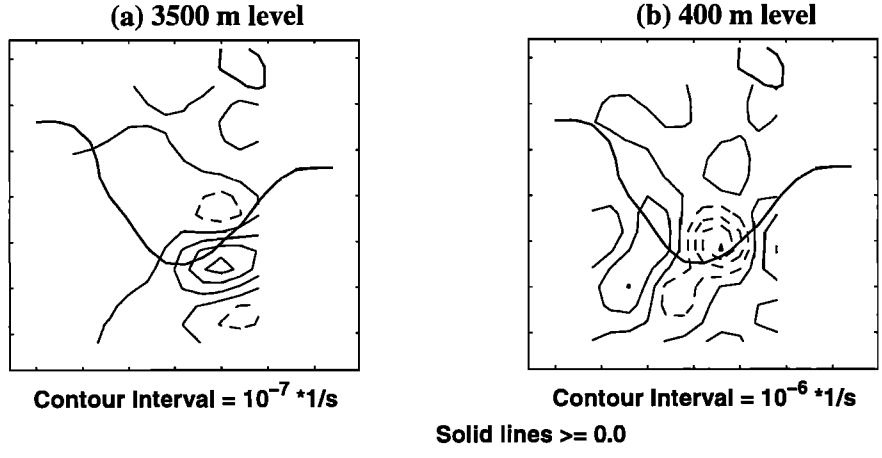

Figure 10. Maps of the right-hand side divergence sum (s^{-1}) over the first 13 days of event A. Maps are for (a) 3500 m and (b) 400 m levels. Positive values indicate convergence and production of positive relative vorticity. Note the difference in contour interval between the two. The bold lines are 400 m depth contours of the 12°Cisothermal surface, indicating the approximate path of the Gulf Stream jet across the array and a warm core ring in the northeastern corner of the array.

5. Vorticity Balance

The vorticity balance during cyclogenesis can be assessed by evaluating terms in the potential vorticity equation, formulated for a two layer ocean. The equation for the subthermocline layer is:

$$\frac{\partial \zeta}{\partial t} + \mathbf{V} \cdot \nabla \zeta = -v\beta + \frac{f_0 + \omega}{(h_i - h_b)} (w_i - w_b) \quad (4)$$

Here ω represents the time varying part of absolute vorticity, $\omega = \zeta + \beta y$, h_i is the depth of the interface between the two ocean layers (the Z6 surface), h_b is the bottom depth, w_i are vertical velocities at the interface, and w_b are vertical velocities at the ocean bottom, resulting from flow across the bottom or from Ekman pumping. Thus ζ can be changed by advection of relative vorticity, advection of planetary vorticity, or vertical stretching of planetary or relative vorticity. Vertical stretching of the water column can result from vertical velocities at the upper limit of the lower layer or from vertical velocities at the ocean bottom.

Layer average horizontal velocities ($\mathbf{V}$), relative vorticity (ζ), and spatial gradients of ζ were calculated as weighted averages of OI quantities from the four measurement levels. The weighting was similar to that used for the crude integration of density in section 3, with the position of the Z6 surface used to determine which portion of the water column should be averaged into the lower layer. For w_i at the Z6 surface, vertical velocities at 700 m were used, calculated using the methods of *Lindstrom et al.* [1997]. The vertical velocity at the bottom, $w_b = \mathbf{V_b} \cdot \nabla h_b + E_{kp}$, where $\mathbf{V_b}$ is horizontal flow at the bottom, and $E_{kp} = \sqrt{A_v/(2f_0)}\zeta_b$ is Ekman pumping (ζ_b is the relative vorticity of flow at the bottom). A ballpark value of $A_v = 10^{-4}$ m^2 s^{-1} was used for the eddy viscosity. This generous value is more consistent with the early estimates of *Munk* [1966] than with more modern microstructure values, which are nearer to $A_v = 10^{-5}$ m^2 s^{-1} [*Gregg*, 1987]. Even so, the Ekman pumping velocities were 2 orders of magnitude smaller than those resulting from flow along the bottom. The relative vorticity (ζ_b) and the horizontal velocity ($\mathbf{V_b}$) were calculated by extrapolating OI velocities at 3500 m to the ocean bottom assuming thermal wind balance and using density gradients at 3500 m, calculated on a uniform grid via OI. Gradients in bathymetry (∇h_b) were calculated using centered finite difference approximations. Temporal derivatives were first differences in time, evaluated over 24 hour increments.

The potential for error in these calculations is large, but a few very general results are evident, based only on sign and relative order of magnitude of the terms. Estimates of the left-hand side terms of Equation (4) show that downstream from Gulf Stream trough axes, the production of positive relative vorticity following a fluid parcel ($D\zeta/Dt$) was primarily due to local changes in relative vorticity, with a small contribution from the advection term. That contribution increases through the developing days of the cyclones. Of the terms on the right-hand side of Equation (4), only water column stretching of planetary vorticity was appreciable. This stretching was due to the large vertical velocities in the main thermocline accompanying large Gulf Stream curvature. Stretching due to bottom vertical velocities was not important. These results are consistent with the scenario suggested by the pressure tendency and divergence equation studies discussed in sections 3 and 4.

Since the production of relative vorticity in the lower layer is primarily forced by water column stretching, the upper layer vorticity balance becomes of interest, in order to diagnose the water column shortening there that must accompany the existence of large positive vertical velocities in the thermocline. Downstream from Gulf Stream trough axes, *Howden* [1996] found a balance between the advection of relative vorticity and stretching of planetary vorticity (in a negative sense) at the upper measurement levels, especially at 700 and 1000 m. This suggests that the production of relative vorticity in the lower layer is directly related to the advection of relative vorticity in the upper layer.

6. Discussion and Summary

The cyclones observed at 3500 m in the SYNOP Central Array, and which extend through the entire water column there, represent one of the fundamental discoveries of the SYNOP observational program. The analysis of the SYNOP cyclones from the perspectives of pressure tendency, divergence, and potential vorticity paints a consistent picture of their dynamics. The cyclones are seen to be nearly geostrophic features associated with low pressure centers located downstream from Gulf Stream meander trough axes. Density field adjustments in the water column above the low pressure center at 3500 m are in the sense to increase pressure at the water column's base, so SSH adjustments must be responsible. The low pressure center may be caused by a depression in sea surface topography that develops as part of the trough amplification process. This depression should have an approximate magnitude of 0.4 m depth over a 250 km horizontal extent (the cyclone's diameter), superimposed on the usual 1 m sea surface rise across the Gulf Stream in the offshore direction. Such a depression results from net divergence in the water column between the low pressure centers observed at 3500 m and the sea surface. Though horizontal convergence is observed in the deep ocean, as expected in association with developing cyclonic flow there, horizontal divergence is observed in the upper ocean downstream from the axes of amplifying meander troughs. This upper-layer divergence is hypothesized to be of sufficient magnitude to over-compensate for the deep-layer convergence, resulting in net divergence in the water column and a locally falling sea surface above the deep low pressure centers. Large positive vertical velocities in the thermocline over developing low pressure centers at 3500 m are consistent with convergence at depth and divergence in the upper ocean. They are also consistent with stretching of the lower water column as seen in the potential vorticity analysis. The stretching of the lower water column accounts for the generation of positive relative vorticity there.

Except for the density field evolution seen here, and its failure to account for the evolving pressure field, the oceanic

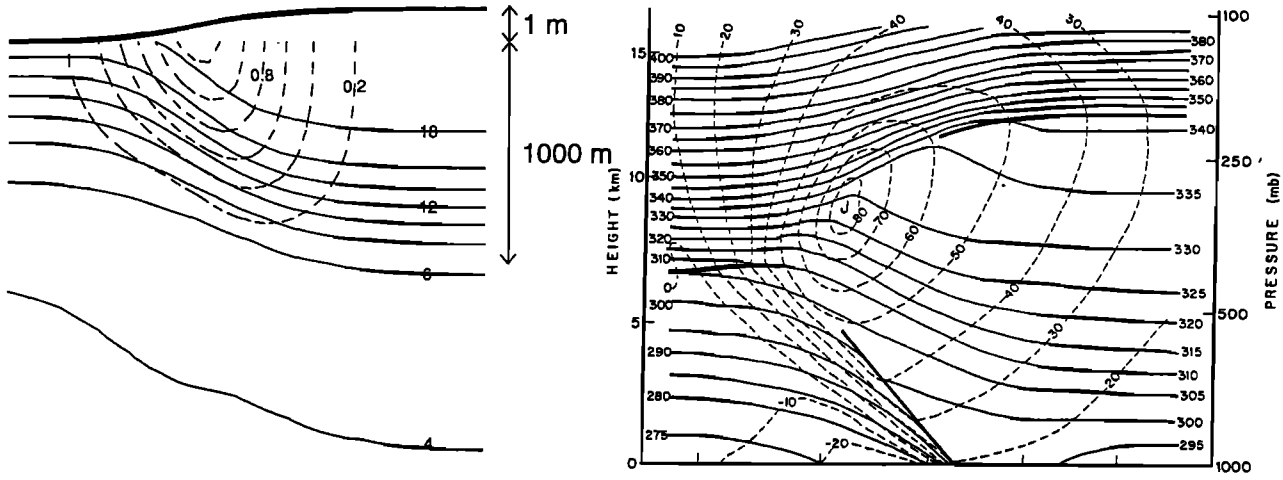

Figure 11. Vertical cross sections through frontal zones for (left) the Gulf Stream and (right) the atmospheric jet stream. Solid lines represent lines of constant potential temperature (°C), dashed lines represent isotachs (m s^{-1}), and the bold solid lines represent the location of the sea surface for the ocean and the tropopause for the atmosphere. The width of the ocean section shown is approximately 150 km. The atmospheric cross section extends from Omaha, Nebraska to Charleston, South Carolina, a distance of approximately 1700 km (Figure 3.20 from *Wallace and Hobbs* [1977], with permission of Academic Press).

case is strikingly similar to the atmospheric case. In fact, the analogy extends even further if the potential density structure of the ocean and atmosphere are considered carefully. The pressure tendency equation for the ocean explicitly considers the large density drop across the ocean surface by the presence of the sea surface variability term (term b in equation (1)). Changes in the slope of that surface can significantly alter subsurface horizontal pressure gradients, as discussed. Though no such interface exists in the atmosphere, the tropopause is characterized by a very large vertical gradient in potential temperature, a good proxy for density (Figure 11). If the integrated density tendency term in the atmospheric case were split into an integration through that layer plus an integration through the rest of the atmosphere, then the tropopause term would likely play a role in the pressure tendancy equation term similar to that played by the sea surface variability term in the oceanic case. Thus changes in the slope of the tropopause would perhaps control horizontal surface pressure gradients. *Fleagle* [1948] points out that the pressure tendency is controlled by advective effects in the upper troposphere and lower stratosphere.

There is some question whether the observed cyclones form preferentially in the region of the SYNOP Central Array. While it is presumed that baroclinic instability in strongly baroclinic currents is possible anywhere, the large amplitude Gulf Stream troughs observed appear in this location often enough to result in a slight trough in the mean Gulf Stream axis placement here [*Shay et al.*, 1995; *Lee and*

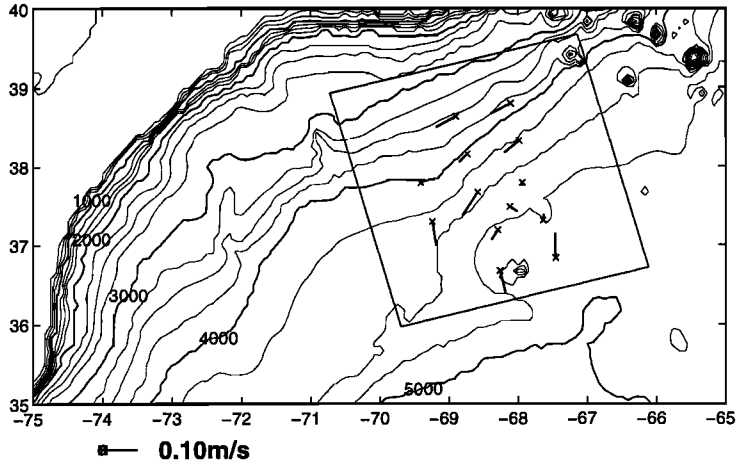

Figure 12. Bathymetry near the SYNOP Central Array. The contour interval is 250 m. Vectors are mean velocities at 3500 m from noncyclone time periods. Mooring locations (crosses) and the area over which thermocline depth was optimally interpolated from IES data (box) are shown.

Cornillon, 1996]. This location is the first place downstream from Cape Hatteras where the Gulf Stream path has crossed seaward of the continental slope and rise and has reached deep water (Figure 12). Since steep bathymetry can suppress baroclinic instability [*Pedlosky*, 1987], the growth of large amplitude meander troughs may be suppressed farther west than the Central Array. Additionally, the New England Seamount Chain is located directly downstream from the Array and may be associated with upstream effects on the Gulf Stream, such as ring generation [*Richardson*, 1983]. As mentioned in the introduction to *Savidge and Bane* [this issue], all of the large amplitude trough and deep cyclone events were coincident with ring-Stream interactions downstream from the SYNOP Central Array. If ring-Stream interactions are a necessary ingredient in the formation of large amplitude meander troughs and if the New England Seamount Chain is indeed associated with ring generation, then their placement immediately downstream from the Central Array may enhance the likelihood of trough amplification and cyclogenesis in the location of the SYNOP Central Array.

Acknowledgments. Much of this work stands on the shoulders of the work of Randy Watts and his group at the Graduate School of Oceanography of the University of Rhode Island. Thanks to Randy, Xiaoshu Qian, Karen Tracey, and Stephan Howden for their input and assistance. Thanks also to Thomas Shay here at UNC-CH for his help and insight. The careful reading and remarks of two anonymous reviewers improved the manuscript substantially. The collection of the SYNOP data was supported by NSF grant OCE-8717141 and by ONR grant N00014-87-K-0233 to the University of North Carolina at Chapel Hill. This analysis of the SYNOP data was supported by NSF grant OCE-9302816 and by ONR grant N00014-92-J-1683 to John Bane at the University of North Carolina at Chapel Hill, by ONR AASERT grant N00014-93-1-1012, and by the Curriculum in Marine Sciences at the University of North Carolina at Chapel Hill.

References

Armi, L., and N. A. Bray, A standard analytic curve of potential temperature versus salinity for the western North Atlantic, *J. Phys. Oceanogr.*, *12*, 384–387, 1982.

Bjerknes, J., and J. Holmboe, On the theory of cyclones, *J. Meteorol.*, *1*, 1–22, 1944.

Bluestein, H. B., *Synoptic-Dynamic Meteorology in Midlatitudes, Vol. 1, Principles of Kinematics and Dynamics*, 431 pp., Oxford University Press, New York, 1992.

Bower, A. S., Potential vorticity balances and horizontal divergence along particle trajectories in Gulf Stream meanders east of Cape Hatteras, *J. Phys. Oceanogr.*, *19*, 1669–1681, 1989.

Charney, J. G., The dynamics of long waves in a baroclinic westerly current, *J. Meteorol.*, *4*, 135–162, 1947.

Cushman-Roisin, B., *Introduction to Geophysical Fluid Dynamics*, 320 pp., Prentice-Hall, Englewood Cliffs, N.J., 1994.

Eady, E. T., Long waves and cyclone waves, *Tellus*, *1*, 33–52, 1949.

Fleagle, R. G., Quantitative analysis of factors influencing pressure change, *J. Meteorol.*, *5*, 281–292, 1948.

Gill, A. E., *Atmosphere-Ocean Dynamics*, 662 pp., Academic, San Diego, Calif., 1982.

Gregg, M. C., Diapycnal mixing in the thermocline: A review, *J. Geophys. Res..*, *92*, 5249–5286, 1987.

Hall, M. M., Horizontal and vertical structure of the Gulf Stream at 68°W, *J. Phys. Oceanogr.*, *16*, 1814–1828, 1986.

He, Y., Determining the baroclinic geostrophic velocity structure with inverted echo sounders, Master's thesis, 135 pp., Univ. of R. I., Kingston, 1993.

Hogg, N. G., Topographic waves along 70°W on the continental rise, *J. Mar. Res.*, *39*, 627–649, 1981.

Holton, J. R., *An Introduction to Dynamic Meteorology*, second ed., 391 pp., Academic, San Diego, Calif., 1979.

Howden, S. D., Processes associated with steep meander development in the Gulf Stream near 68°W, Ph.D. thesis, 229 pp., Univ. of R. I., Kingston, 1996.

Lee, T., and P. Cornillon, Propagation and growth of Gulf Stream meanders between 75°and 45°W, *J. Phys. Oceanogr.*, *26*, 225–241, 1996.

Lindstrom, S., X. Qian, and D. R. Watts, Vertical motion in the Gulf Stream and its relation to meanders, *J. Geophys. Res.*, *102*, 8485–8503, 1997.

Luyten, J. R., Scales of motion in the deep Gulf Stream and across the continental rise, *J. Mar. Res.*, *35*, 49–74, 1977.

Morgan, P. P., SEAWATER: A library of MATLAB computational routines for the properties of seawater, *Tech. Rep. 222*, Commonwealth Sci. and Ind. Res. Org. Marine Laboratories, Hobart, Australia, 1994.

Munk, W., Abyssal recipes, *Deep Sea Res.*, *13*, 707–730, 1966.

Palmen, E., and C. W. Newton, *Atmospheric Circulation Systems*, first ed., 603 pp., Academic, San Diego, 1969.

Pedlosky, J., *Geophysical Fluid Dynamics*, 2nd ed., 710 pp., Springer-Verlag, New York, 1987.

Richardson, P. L., Gulf Stream rings, in *Eddies in Marine Science*, edited by A. Robinson, pp. pp. 19–45, Springer-Verlag, New York, 1983.

Rossby, T., On the energetics of the Gulf Stream at 73°W, *J. Mar. Res.*, *45*, 59–82, 1987.

Rossby, T., and E. Gottlieb, The Oleander Project: Monitoring the variability of the Gulf Stream and adjacent waters between New Jersey and Bermuda, *Bull. of Am. Meteorol. Soc.*, *79*, 5–18, 1998.

Savidge, D. K., and J. M. Bane, Cyclogenesis in the deep ocean beneath the Gulf Stream 1. Description, *J. Geophys. Res.*, this issue.

Savidge, D. K., T. J. Shay, and J. M. Bane, Synoptic Ocean Prediction Experiment: EN216 CTD section data report, *Tech. Rep. CMS93-1*, Univ. of N. C., Chapel Hill, 1993.

Shay, T. J., J. M. Bane, D. R. Watts, and K. L. Tracey, Gulf Stream flow field and events near 68°W, *J. Geophys. Res.*, *100*, 22,565–22,589, 1995.

Wallace, J. M., and P. V. Hobbs, *Atmospheric Science, An Introductory Survey*, 467 pp., Academic, San Diego, Calif., 1977.

J. M. Bane Jr. and D. K. Savidge, Department of Marine Sciences, University of North Carolina at Chapel Hill, CB# 3300 Venable Hall, Chapel Hill, NC, 27599. (dana@marine.unc.edu

(Received December 18, 1997; revised March 12, 1999; accepted March 24, 1999.)